Contents lists available at ScienceDirect

Food and Bioproducts Processing

journal homepage: www.elsevier.com/locate/fbp

Picosecond laser treatment production of hierarchical structured stainless steel to reduce bacterial fouling

Fatema H. Rajab[a], *Christopher M. Liauw*[a], *Paul S. Benson*[b], *Lin Li*[a], *Kathryn A. Whitehead*[b,*]

[a] *Laser Processing Research Centre, School of Mechanical, Aerospace and Civil Engineering, The University of Manchester, Manchester M13 9PL, UK*

[b] *Microbiology at Interfaces Group, School of Healthcare Science, Manchester Metropolitan University, Manchester M1 5GD, UK*

ARTICLE INFO

Article history:
Received 1 October 2017
Received in revised form 1 February 2018
Accepted 26 February 2018
Available online 10 March 2018

Keywords:
Picosecond laser
Bacteria
Superhydrophobic
Topography
Biofouling
Food industry

ABSTRACT

The design of surfaces that prevent biofouling through their physical structure and chemical properties provides a potential solution to increase their hygienic status. A picosecond laser was used to produce hierarchical textures on stainless steel. The surface topography, chemistry and wettability were characterised. The S_a, and wettability of the surfaces all increased when compared to the control following laser treatment. The S_a, S_q and S_{pv} values ranged between 0.02 μm–1.16 μm, 0.02 μm–1.30 μm and 0.82 μm–9.84 μm respectively whilst the wettability of the surfaces ranged between 99.5°–160°. Following microbial assays, the work demonstrated that on all the surfaces, following attachment, adhesion and retention assays, the number of *Escherichia coli* on the laser textured surfaces was reduced. One surface was demonstrated to be the best antiadhesive surface, which alongside being superhydrophobic (154.30°) had the greatest S_a and S_{pv} (1.16 μm; 6.17 μm) values, and the greatest peak (21.63 μm) and valley (21.41 μm) widths. This study showed that the surface roughness, feature geometry, chemistry and physicochemistry all interplayed to affect bacterial attachment, adhesion and retention Such a modified stainless steel surface may have the ability to reduce specific fouling in an industrial context.

1. Introduction

Biofouling on surfaces can produce a number of economic and potential contamination problems in a variety of industries including the food industry (Whitehead and Verran, 2009). Bacterial attachment is the prerequisite to such fouling and is followed by bacterial adhesion and retention on a surface. This may result in the decline of the hygienic status of a surface resulting in potential risks to food quality, product contamination and/or spoilage and blockages of mechanical components (Whitehead et al., 2015). In 2011, it was reported that foodborne disease caused a projected 48 million illnesses, 128,000 hospitalisations and 3000 deaths annually in United States between 1996 and 2010 (Nyachuba, 2010; Schlisselberg and Yaron, 2013; Srey et al., 2013).

The modification of substratum topography, chemistry and/or physicochemistry can be used to reduce microbial biofouling. Many studies have been carried out to determine the effect of surface properties on bacterial attachment and retention (Hilbert et al., 2003; Jullien et al., 2003; Whitehead et al., 2005; Whitehead and Verran, 2006; Wang et al., 2009; Milledge, 2010; Dantas et al., 2016; Tetlow et al., 2017). Some studies have reported that there is a correlation between surfaces roughness and bacterial attachment whereby the retention of

* *Corresponding author.*
E-mail address: K.A.Whitehead@mmu.ac.uk (K.A. Whitehead).
https://doi.org/10.1016/j.fbp.2018.02.009

microorganisms increased with increasing surface roughness (Jullien et al., 2003; Wang et al., 2009; Whitehead et al., 2011; Dantas et al., 2016). However, others have reported that there was little or no relationship between surface roughness and bacterial attachment (Hilbert et al., 2003; Milledge, 2010). The effect of surface wettability on bacterial attachment has also been carried out and it has been reported that the number of adhered bacteria was dramatically decreased with increasing surface hydrophobicity and bacteria adhered to hydrophobic materials were more easily removed by an increased flow or an air-bubble jet (Bos et al., 2000; Fadeeva et al., 2011; Privett et al., 2011; Dou et al., 2015). However, others have reported that there was no relationship between surface wettability and bacterial attachment (Cunha et al., 2016).

Surface topographies can be grouped into three main structural types namely irregular, regular or hierarchical. Although changes in the surface topography are usually described using the average roughness value (R_a), it has been suggested that an in depth evaluation of the shape of the surface features also needs to be described (Whitehead et al., 2005). Several studies have been carried out to study the effect of topographies, for example grooves (Verran et al., 2010), squared-features (Perera-Costa et al., 2014) or pits (Whitehead et al., 2005; Whitehead and Verran, 2006). In nature, there are many plants with hierarchical surface structures that are considered as self-cleaning surfaces such as the lotus leaf. These surfaces are superhydrophobic with contact angles ≥150° and sliding angles <5° (Yan et al., 2011). Several studies of bacterial attachment and retention on such biomimetic type features for example those which replicate the lotus leaf (Fadeeva et al., 2011) or taro leaf (Crick et al., 2011) have been carried out.

Stainless steel is a used in a wide range of industrial applications due to its unique properties such as ease of fabrication and modification, corrosive resistance, inertness and ease of cleaning. Different techniques such as lithography (Gold et al., 1995), moulding (Chou et al., 1995) and photolithography (Green et al., 1994) have been used to produce different micro/nano structures, but most of these are not compatible with stainless steel surfaces. Laser surface modification has been extensively studied for the production of surfaces to be used in a range of different applications (Dobrzański et al., 2008; Cunha et al., 2013; Long et al., 2016, 2015b). This paper focuses on the production of a range of hierarchical (macro/micro/nano) topographies generated using a novel picosecond laser ablation process and the effect of the altered surface properties on bacterial attachment, adhesion and retention.

2. Material and methods

2.1. Laser surface texture preparation

Stainless steel surfaces (316L, S_a 20 nm ± 0.1 nm finish) with a 0.7 mm thickness was used in this work to produce laser etched areas 5 mm × 5 mm in size. Before laser treatment, the surfaces were cleaned ultrasonically with acetone followed by ethanol then deionised water for 10 min each. The experiment was performed using an EdgeWave Nd:YVO_4 picosecond laser of 10 ps pulse duration, with a 103 kHz repetition rate, 1.06 μm, 125 μm beam size in ambient air using a range of scanning parameters (Table 1). The scanning was performed using either parallel or cross lines patterns. After laser treatment, the surfaces were cleaned ultrasonically with ethanol for 5 min then dried using compressed air for 5 s–10 s to remove any ablated debris or contamination. The surfaces were immersed into a 1% hetadecafluoro-1,1,2,2-tetrahydrodecyl-1-trimethoxysilane ($CF_3(CF_2)_7(CH_2)2Si(OCH_3)_3$) (Gilest Inc., USA), (referred to as FSA) methanol solution for 2 h followed by rinsing with ethanol and drying in an oven at 80 °C for 30 min (Long et al., 2015a).

2.2. Surface characterization

After laser treatment, the macrostructure of the surfaces was imaged using a scanning electron microscope (SEM) (Carl Zeiss Ltd. UK). The microtopography and roughness values of the surfaces were also characterised using laser profilometry (Keyence, UK). Values of S_a (Arithmetic mean height), S_q (Root mean square height) and S_{pv} (Maximum height of the surface) were recorded for each of the surfaces. Selected line scans were used to determine the height, depth and width of the peaks and valleys. Atomic force microscopy (Veeco Instruments Inc., UK) was used to examine the nanotopography of the surfaces. Image processing was carried out using the Scanning Probe Image Processor. Selected line scans were used to determine the height, depth and width of the peaks and valleys. Chemical analysis was carried out using Energy Dispersive X Ray (EDX) on the SEM instrumentation (n = 3).

2.3. Confocal laser microscopy (CSLM) and atomic force microscopy (AFM)

For CSLM, the surfaces were examined using a 150× objective (Keyence X200K 3D Confocal Laser Microscope, USA with VK analyser software) to determine the substratum macro and micro topographies. The S_a, S_q and S_{pv} (average surface roughness, root-mean square roughness and peak to valley height respectively) was measured for the surfaces. To determine the shape height, depth and width of the peaks and valleys line profiles were used.

AFM measurements were carried out to determine the nanotopographies of the surfaces using a Dimension 3100 AFM (Veeco Instruments Inc., UK).

2.4. Physicochemistry

The physicochemistry of the surfaces was obtained by measuring the contact angle via the sessile drop method (FTA 188, UK). By measuring contact angles for three fluids with known γ_L values, the three variables, γ_s^{LW}, γ_S^+ and γ_S^- could be determined (n = 10). Six microliter droplets of deionised water, formamide or α-bromonaphthalene were dropped onto the surface. The approach of Van Oss et al. (1989) was used to calculate the surface hydrophobicity. The degree of hydrophobicity of the surfaces was expressed as the surfaces free energy of interaction of the material when immersed in water (w) (ΔG_{iwi}). The material was considered hydrophobic when the surface $\Delta G_{iwi} < 0$ and hydrophilic when $\Delta G_{iwi} > 0$. ΔG_{iwi} was calculated according to Eq. (1) (Van Oss et al., 1989),

$$\Delta G_{iwi} = -2\gamma_{sL} \quad (1)$$

The SFE (γ_s) was determined from the polar or Lewis acid base component (γ_s^{AB}) and apolar Lifshitz–van der Waal component (γ_s^{LW}) where;

$$\gamma_s = \gamma_s^{LW} + \gamma_s^{AB} \quad (2)$$

where γ^{LW} was the Lifshitz–van der Waals component of the surface free energy and the Lewis acid–base component γ^{AB}.

γ_s^{AB} was calculated from;

$$\gamma_s^{AB} = 2\sqrt{\gamma^+\gamma^-}. \quad (3)$$

Table 1 – Laser processing parameters used to produce the different surface topographies.

	Texture	Fluence (J/cm^2)	Scanning speed (mm/s)	Hatch distance (μm)	Scanning
Control	316 stainless steel	N/A	N/A	N/A	N/A
SS1	Small rounded irregular shaped and sized features with grooves	0.18	10	10	1 day
SS2	Large rounded irregular shaped and sized features with grooves	0.18	10	10	1 day (30°)
SS3	Narrow linear features with nano particles unevenly distributed across the tops of the surfaces, LIPPS	0.18	10	100	1 day
SS4	Linear with irregularly clustered hair like projections	0.13	1000	50	2 day
SS5	Elongated rounded shapes with irregular linear grooves and hair like structure	0.13	10	10	1 day

where γ_s^+ is the electron acceptor and γ_s^- is the electron donor of the polar surface tension component. The apolar components of the liquid and surface were combined;

$$\gamma_{sL}^{LW} = \left(\sqrt{\gamma_S^{LW}} - \sqrt{\gamma_L^{LW}}\right)^2 \quad (4)$$

The polar components were calculated from;

$$\gamma_{sL}^{AB} = 2\left(\sqrt{\gamma_s^+\gamma_s^-} + \sqrt{\gamma_L^+\gamma_L^-} - \sqrt{\gamma_s^+\gamma_L^-} - \sqrt{\gamma_s^-\gamma_L^+}\right) \quad (5)$$

The surface free energy values can be calculated by;

$$\gamma_L(1+\cos\theta) = 2\left(\sqrt{\gamma_s^{LW}\gamma_L^{LW}} + \sqrt{\gamma_s^+\gamma_L^-} + \sqrt{\gamma_s^-\gamma_L^+}\right) \quad (6)$$

2.5. Microbiology

One hundred millilitres of nutrient broth (Oxoid, UK) was inoculated with a single colony of *Escherichia coli* NCTC 9001 and incubated at 37 °C overnight for 24 h. Following incubation, cells were harvested at 3500 rpm for 10 min and were washed and re-suspended using 10 mL sterile distilled water three times. Cells were re-suspended to Optical Density (OD) 1.0 ± 0.1 at 540 nm in sterile distilled water. Serial dilutions were used to determine the colony-forming units/mL (cfu/mL) and were 2.83×10^9 cfu/mL.

2.5.1. Spray with wash (attachment) and spray (adhesion) assays

In order to determine the attachment (spray with wash assay) or adhesion (spray assay) of the bacteria to the surfaces, two microbiological assays were carried out. Three replicates of the textured or control surfaces were attached to a stainless steel tray using adhesive gum. Bacterial suspension (OD 1.0 @ 540 nm) was placed into the spray reservoir of a Badger Airbrush (Shesto, UK), propelled by a Letraset 600 mL liquid gas canister (Esselte Letraset Ltd., UK). The surfaces were placed vertically in a class 2 flow hood. At a distance of 10 cm, the airbrush was sprayed over the substrate for 10 s. Immediately after spraying, the surfaces were divided into two sets, one was laid horizontally and left to dry (spray assay, adhesion) and other were rinsed gently with distilled water using distilled water bottle at 45° angle of 3 mm nozzle and were dried for 1 h at room temperature (spray with wash assay – attachment). The surfaces were then prepared for SEM imaging (n = 15).

2.5.2. Retention assays

To determine how the bacteria were retained on the surfaces, microbial retention assays were carried out. Newly prepared surfaces were placed in sterile Petri dishes and 25 mL of cell suspension at OD 1.0 ± 0.1 was added. The surfaces were incubated without agitation for 1 h. The surfaces were washed gently with 10 mL distilled water using distilled water bottle at 45° angle, with a 3 mm nozzle. The surfaces were dried in a laminar flow hood for 1 h and then were prepared for SEM examination. The experiments were performed in triplicate. Five images of each surface with the retained bacteria were taken. Then the number of attached cells for each image was counted (n = 15).

2.5.3. Preparation of microbial surfaces for SEM

After drying the surfaces with cells, the coupons were immersed in 4% glutaraldehyde overnight at 4 °C in order to fix the bacterial cells. The surfaces were thoroughly rinsed with 10 mL distilled water using a distilled water bottle at 45° angle of 3 mm nozzle. They were dried for 1 h in a class 2 flow hood then they were immersed for 10 min in different concentrations of absolute ethanol (30%, 50%, 70%, 90% and 100%) and dried for 1 h. The surfaces with retained bacteria were attached to SEM stubs with carbon tabs prior to being sputter coated with a gold and palladium coating (Model: SC7640, Polaron, Au/Pd target, deposition time: 1.5 min). SEM was carried out using a Supra 40VP with SmartSEM software (Carl Zeiss Ltd. UK). All the images were taken at 15,000× magnification.

2.6. Statistics

The statistical test used a two-sample student's t-test. The data were considered significant at $p < 0.05$. Error bars indicate the standard error of the data.

3. Results

The surfaces were characterised in terms of macro, micro, nano-topographies, and physicochemistries in order to determine their influence on bacteria attachment, adhesion and retention.

3.1. Laser surface texturing

Picosecond (Ps) laser ablation was used to fabricate hierarchical structures on stainless steel (Table 1). SEM (Fig. 1) was used to determine the overall surface feature differences and CSLM (Figs. 2 and 3/Table 2) was used to quantify the surface features

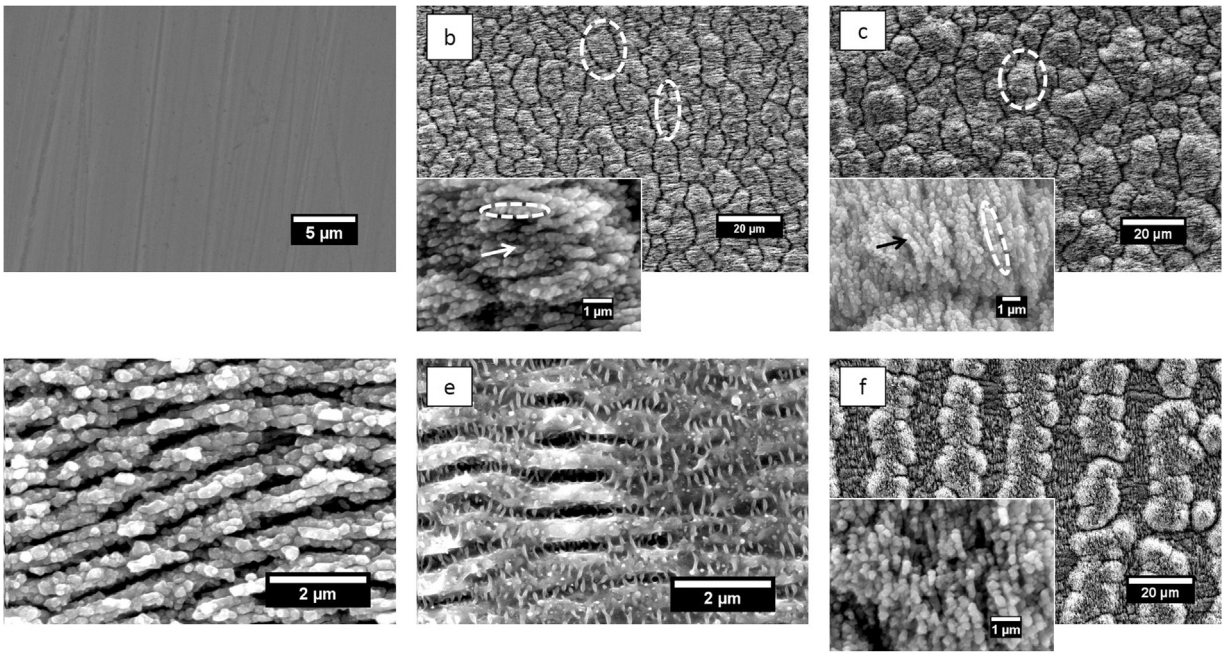

Fig. 1 – SEM images demonstrating the macro topography of the different surface features: (a) control, (b) SS1, (c) SS2, (d) SS3, (e) SS4, and (f) SS5. Inserts demonstrate increased magnifications of the surface topographies.

Table 2 – Maximum width and height of the surface features (standard deviations are in parenthesis).

	Max peak width (µm)	Max peak height (µm)	Max valley width (µm)	Max valley depth (µm)
Control	3.61 (0.7)	0.06 (0.1)	1.24 (0.5)	0.09 (0.5)
SS1	9.77 (0.6)	3.19 (0.1)	16.0 (3.3)	3.38 (0.6)
SS2	20.0 (1.0)	4.34 (0.8)	19.9 (0.6)	4.70 (0.7)
SS3	3.70 (1.0)	0.53 (0.1)	3.15 (0.7)	0.48 (0.1)
SS4	2.30 (0.4)	0.13 (0.1)	1.90 (1.4)	0.17 (0.1)
SS5	21.6 (2.6)	4.24 (0.2)	21.4 (2.5)	4.93 (0.3)

Table 3 – Average width and height of the surface features using AFM (standard deviations are in parenthesis).

	Average peak width (µm)	Average peak height (µm)	Average valley width (µm)	Average valley depth (µm)
Control	0.09 (0.05)	0.01 (0.01)	0.09 (0.05)	0.01 (0.01)
SS1	0.29 (0.18)	0.12 (0.13)	0.19 (0.10)	0.10 (0.09)
SS2	0.30 (0.20)	0.10 (0.04)	0.22 (0.08)	0.12 (0.07)
SS3	0.14 (0.06)	0.04 (0.03)	0.15 (0.08)	0.04 (0.03)
SS4	0.11 (0.04)	0.02 (0.01)	0.13 (0.05)	0.02 (0.01)
SS5	0.19 (0.10)	0.06 (0.07)	0.12 (0.10)	0.06 (0.07)

at the macro/micro scale and the S_a, S_q and S_{pv} values. AFM was used to quantify and describe the nano-topographies of the surfaces following Ps laser treatment (Figs. 5 and 6 and Table 3). The shape and size of the different surface features were dependent on the laser parameters used.

3.1.1. *Macro and micro topographies*

The SEM images (Fig. 1) demonstrated that the macro topographies showed that the control surface had the least surface roughness with some lines irregularly distributed across the surface (Fig. 1a) whilst the other surfaces demonstrated a range of features (Fig. 1b–f; Table 1). Using CSLM it was observed that the control surface demonstrated the least micro surface features (Fig. 2a) and from the profilometry images had a nano-roughness with a waviness of form (Fig. 3a). This was quantified (Table 2) and in agreement with the qualitative observations, the maximum peak width (3.61 µm), maximum peak height (0.06 µm), maximum valley width and depth (1.24 µm and 0.09 µm respectively) all gave the lowest values. Overall surfaces SS1, SS2 and SS5 were significantly different to the other surfaces ($p > 0.05$). The surface values confirmed the surface topography data for the control surface the S_a (0.02 µm), S_q (0.02 µm) and S_{pv} (0.82 µm) values were the lowest recorded and was significantly different to the other surfaces (Fig. 4).

The SS1 and SS2 surfaces that were produced using a hatch distance of 10 µm, 10 mm/s and 0.178 J/cm^2 (Fig. 1b, c) demonstrated that at the macro scale, the surfaces had rounded, but irregularly shaped small (Fig. 1b) or larger (Fig. 1c) topographies (white dotted lines) separated with microgrooves which were covered with dual scale patterns (LIPSS) and small particles. CLSM showed that at the micro scale, the SS1 surface had irregularly shaped and spaced bumpy shaped peaks (Fig. 2b) while SS2 (Fig. 2c) demonstrated marginally larger peaks compared with SS1. The 2D profilometry image of SS1 (Fig. 3b) demonstrated a closely formed rounded peaks, whilst SS2 (Fig. 3c) demonstrated marginally larger and rounded peaks than SS1. Data quantification (Table 2) illustrated that SS2 had a higher maximum peak width (20.00 µm), maximum peak height (4.34 µm), maximum valley width (19.68 µm) and

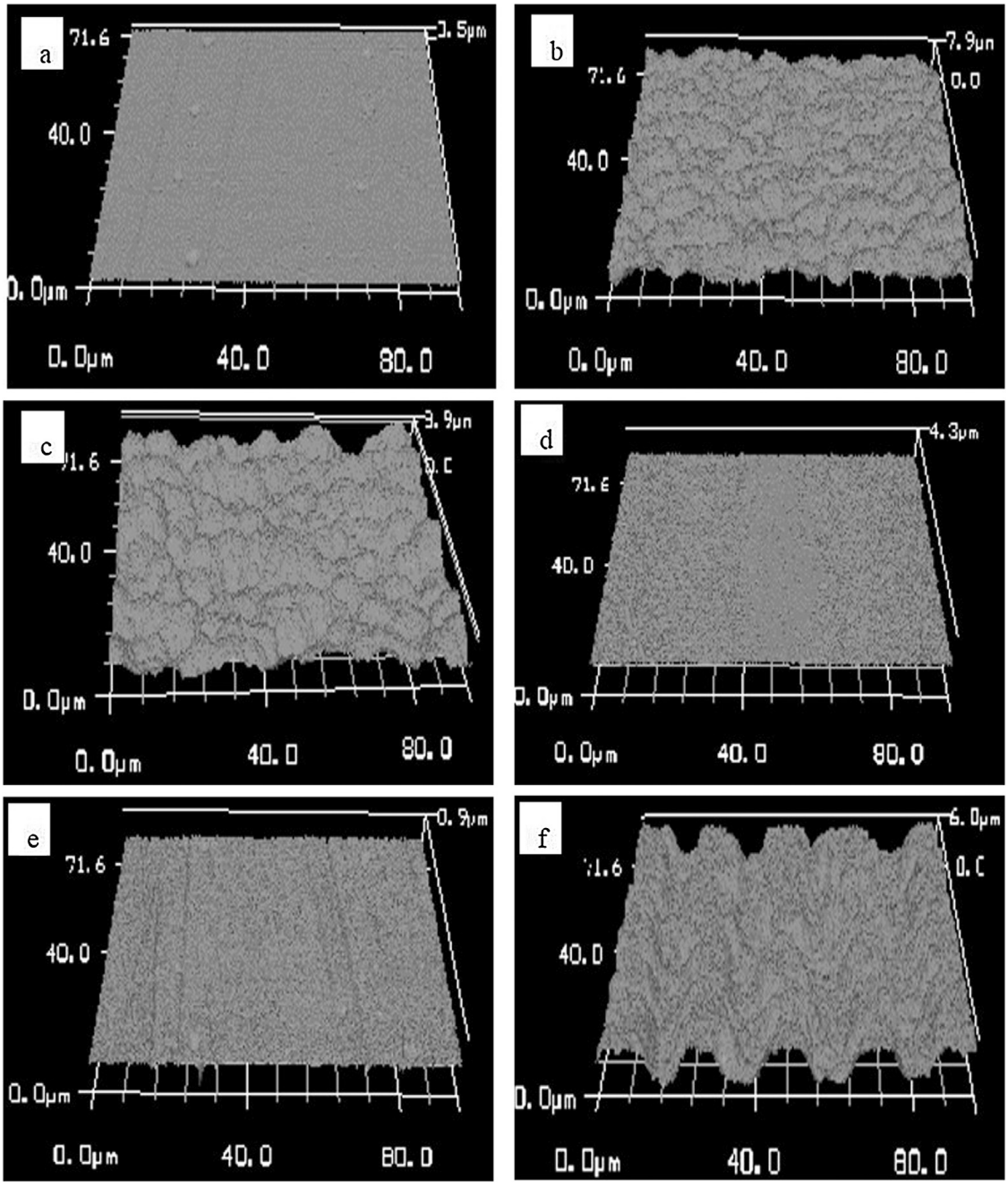

Fig. 2 – Confocal laser microscope images demonstrating micro topography of the surfaces produced using laser treatment: (a) control, (b) SS1, (c) SS2, (d) SS3, (e) SS4, and (f) SS5.

maximum valley height (4.70 µm) compared with SS1 that had surface feature values of 9.77 µm maximum peak width, 3.19 µm maximum peak height, 15.99 µm maximum valley width and 3.38 µm maximum valley height. The surface values confirmed the surface topography data for the SS1and SS2 surfaces. The S_a, S_q and S_{pv} values were 0.69 µm 0.87 µm, 0.73 µm and 1.05 µm 1.3 µm and 1.1 µm respectively. The SS2 surface demonstrated the greatest S_{pv} value when a comparison of all the laser textured surfaces was made (Fig. 4). The S_a, and S_q values were for SS1, SS2 and SS5 were significantly different to the other surfaces ($p > 0.05$). All the surfaces demonstrated significantly different S_{pv} values when compared to the control surface.

The SS3 surface was produced using a laser speed of 10 mm/s with high hatch distance of 100 µm. This resulted in a surface topography with narrow linear features with nano (<0.5 µm) particles unevenly distributed across the tops of the surfaces (Fig. 1d). CLSM demonstrated that at the micron scale, the SS3 had short grass like structures covering the surfaces (Fig. 2d) and 2D profilometry quantification demonstrated smaller surface features compared with all the other laser textured surfaces (Fig. 3d). This was quantified (Table 2) with the maximum peak width (3.70 µm), maximum peak height (0.53 µm), maximum valley width and depth (3.15 µm and 0.43 µm respectively) demonstrating smaller surface features for the SS3 surface with the exception of the control and SS4 surface. It was demonstrated that a S_a and S_q value was obtained that was similar to that of control (0.08 µm and 0.11 µm respectively). However, it demonstrated that the greatest S_{pv} (2.67 µm) was obtained than that of the control (Fig. 4).

The SS4 surface was produced using a high scanning speed of 1000 mm/s which resulted in a linear surface topography with irregularly clustered hair like projections (Fig. 1e). Results

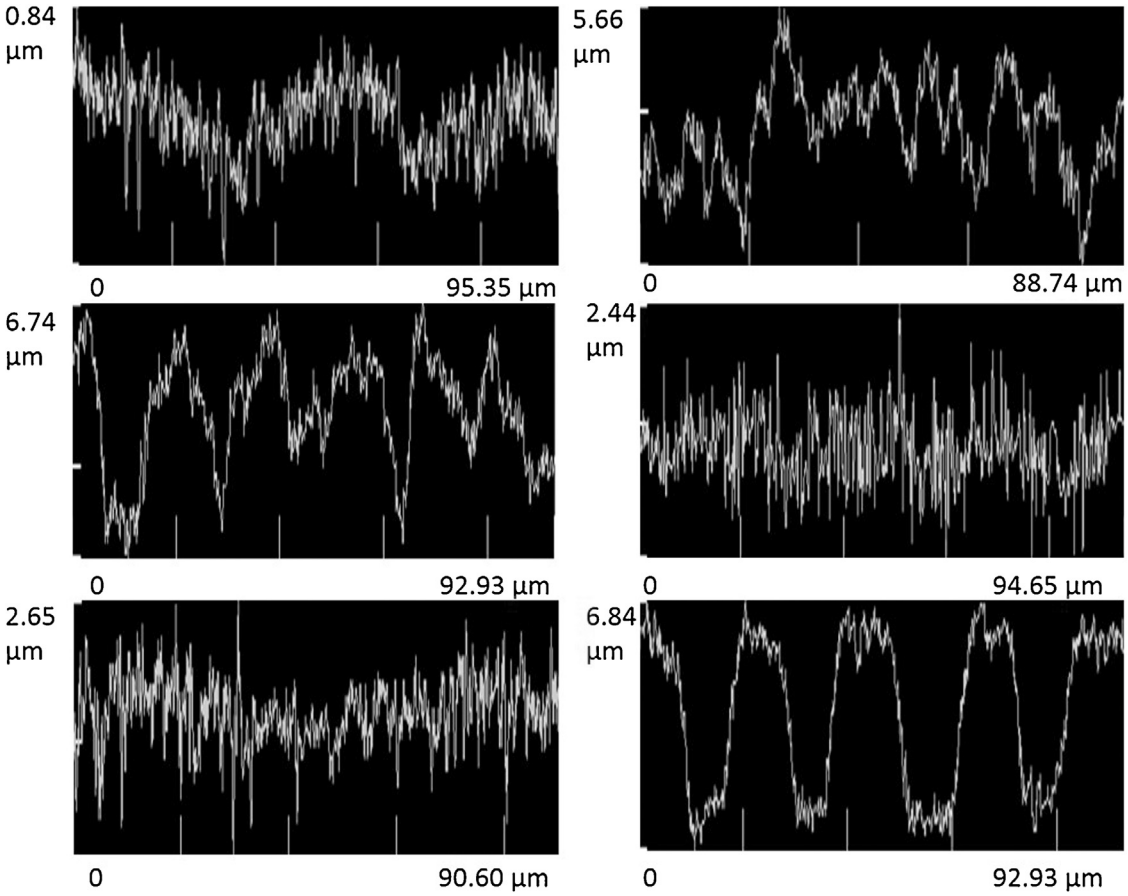

Fig. 3 – Corresponding surface profiles to the images in Fig. 2 demonstrating the size of the different micro surface features: (a) control, (b) SS1, (c) SS2, (d) SS3, (e) SS4, and (f) SS5.

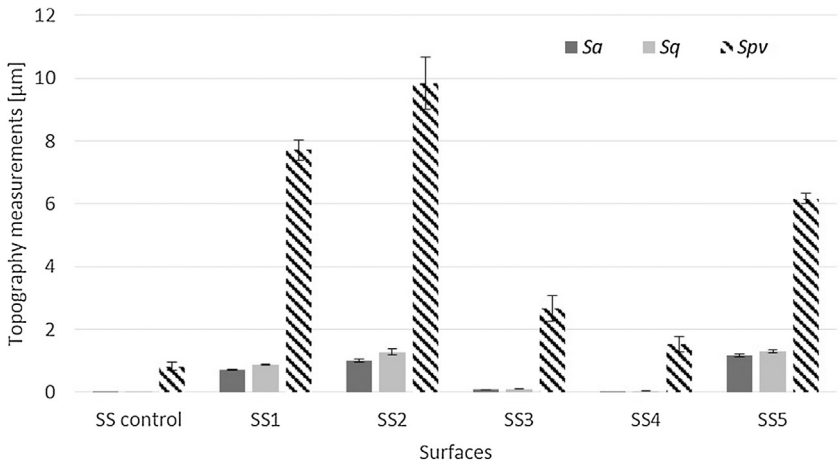

Fig. 4 – Surface topography values S_a, S_q and S_{pv} obtained using CSLM for the laser etched stainless steel surfaces.

from the CSLM, demonstrated that at the micro scale, the SS4 surface was irregular and spiky in appearance (Fig. 2e). Line profilometry demonstrated the least differences in surface features when compared to the control and it was of narrower linear features (Fig. 3e) with the maximum peak width (2.30 µm), maximum peak height (0.13 µm), maximum valley width and depth (1.90 µm and 0.17 µm respectively) confirming the smallest surface features. The S_a and S_q values (0.02 µm and 0.04 µm) were similar to that of control surface while the S_{pv} (1.53 µm) was higher compared with that of control (Fig. 4).

When the surfaces were produced at a laser speed of 10 mm/s and 10 µm but with low laser fluence than for SS5, the surface demonstrated elongated, rounded peaks with irregular shaped groove covered by liner hair like structures. SS5 (Fig. 3f) had a linear pattern of rounded topped surface features and demonstrated intermediary vales for the peak width (0.19 µm), peak height (0.06 µm) and valley width (0.12 µm) and depth (0.06 µm) of all the surfaces. This was the roughest laser textured surface with the intermediary S_a (1.16 µm) and S_q (1.30 µm) values (Fig. 4). The S_{pv} value was 6.17 µm. For the micro surface features, surfaces SS1, SS2 and SS5 were significantly different to the other surfaces ($p > 0.05$).

3.1.2. *Nano topographies*

AFM was used to determine the nano-features of the laser etched surfaces (Figs. 5 and 6). The results demonstrated that the nano-features for the SS3 and SS4 surfaces were more rounded in shape with sharp peaks like spikes than for the SS1,

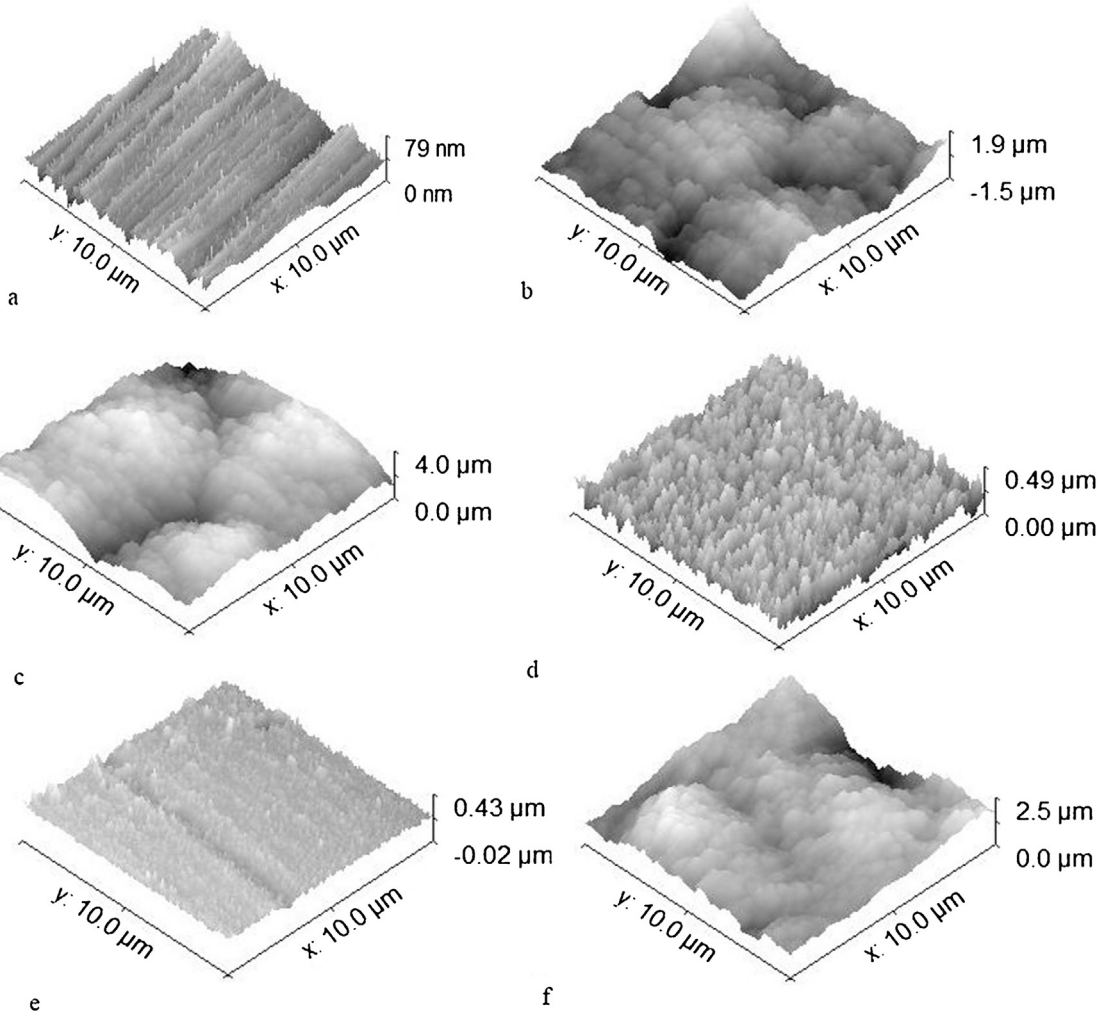

Fig. 5 – AFM images of the different surface nano features: (a) control, (b) SS1, (c) SS2, (d) SS3, (e) SS4, and (f) SS5.

Table 4 – Description of the shape of the macro, micro and nano surface topography features.

	Macro	Micro	Nano
Control	Flat and smooth with some lines irregularly distributed on the surfaces.	Irregular and parallel striations of 3.6 μm width and 60 nm height.	Strips of Peaks of 90 nm width and 0.2 nm height.
SS1	Elongated bumpy structure separated with microgrooves and covered with dual scale patterns (LIPSS)	Irregular rounded peaks with peaks width of 9.77 μm and 3.19 μm height.	Rounded particles of peaks of 290 nm and 120 nm height.
SS2	Elongated bumpy structure separated with microgrooves and covered with dual scale patterns (LIPSS)	Irregular rounded peaks of 20 μm width and 4.3 μm heights.	Rounded particles of peaks of 300 nm and 100 nm height.
SS3	Narrow linear features of size around 1 μm with (<0.5 μm) particles unevenly distributed across the tops of the surfaces.	Short grass like features of peak width 3.7 μm and 0.53 μm with lined in strips.	Sharp peaks like spikes of 140 nm width and 40 nm height.
SS4	Linear topography with irregularly clustered hair like projections.	Irregular and bumpy in appearance with peaks width 2.30 μm and height 0.13 μm.	Sharp peaks like spikes of 110 nm width and 20 nm height.
SS5	Rounded shaped peaks separated with irregular spaces and covered with small particles of hair like structures.	Regularly sized, but irregularly spaced rounded peaks with peak of 21.6 μm width and 4.24 μm height, distributed in a linear fashion, with clear valleys between the rows of peaks.	Rounded particles of peaks of 190 nm and 60 nm height.

SS2 and SS5 surfaces. Moreover, the surface features for the SS2 surface in terms of the peak width and height and valley depth and width were of the largest sizes values and SS4 was of small features (Table 3). The control surface demonstrated linear strips (Fig. 5a) with irregularly spaced peaks (Fig. 6a). It demonstrated that the lowest peaks width was 0.09 μm, peaks heights 0.002 μm, lowest valley width 0.09 μm and lowest valley depth 0.002 μm (Table 3). SS1 and SS2 were covered with

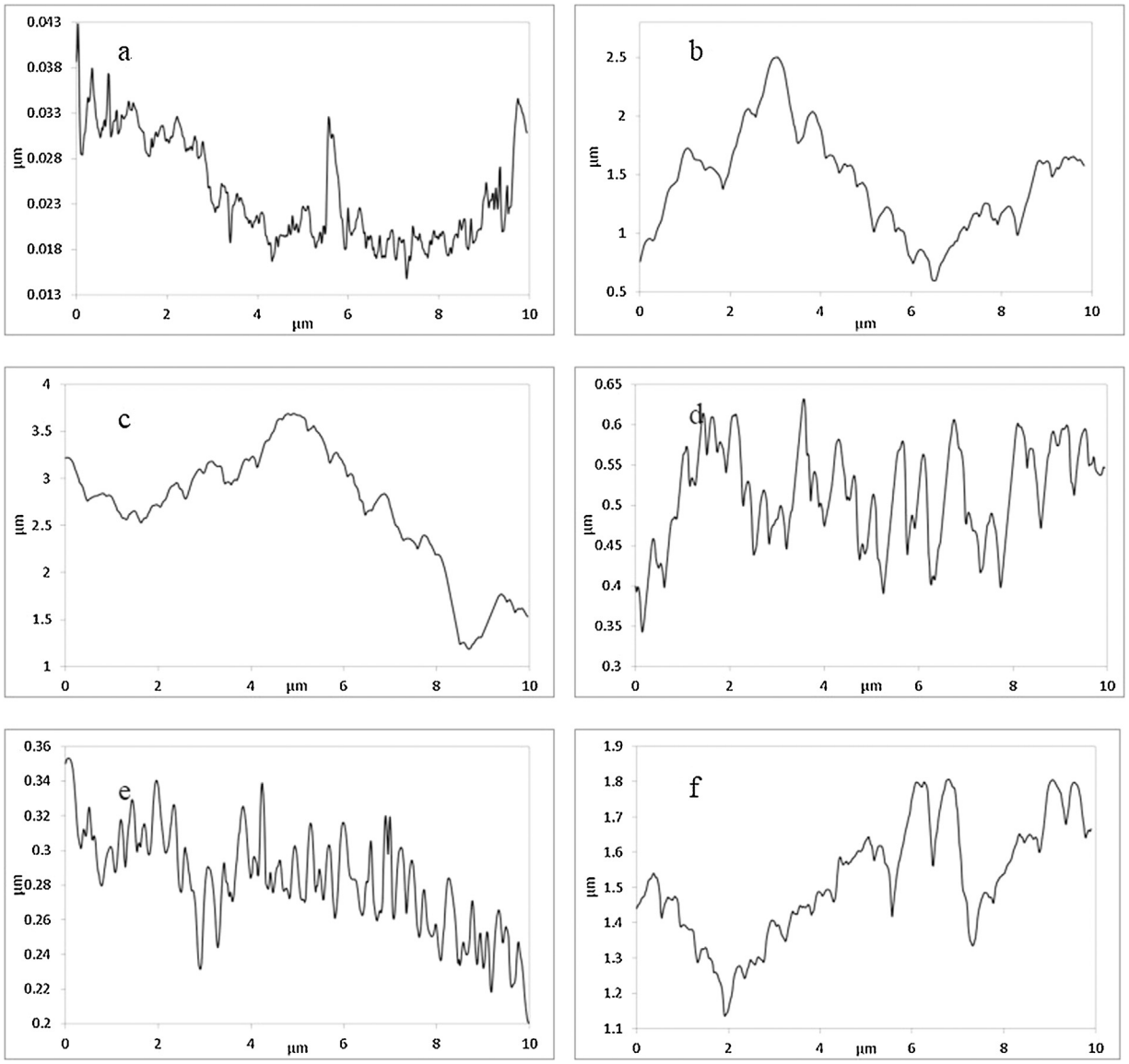

Fig. 6 – Surface profiles of AFM images demonstrating the size and shape of the nano surface features: (a) control, (b) SS1, (c) SS2, (d) SS3, (e) SS4, and (f) SS5.

rounded particles (Fig. 5b and c). The particles that covered SS2 were smaller in appearance (Fig. 5c) and less sharp (Fig. 6c) than those of SS1 (Figs. 5b and 6b). The peak width and height and valley width and depth of both surfaces were nearly same (Table 3). The values were peak width (0.29 µm, 0.30 µm) and height (0.12 µm, 0.10 µm) and valley width (0.19 µm, 0.22 µm) and depth (0.10 µm, 0.12 µm) of (SS1, SS2) respectively. SS3 and SS4 were covered with irregularly spaced, sharp spiky peaks (Figs. 5d and 6d). The peak width and height and valley width and depth of both surfaces were mot significantly different (Table 3). However, SS4 had a smaller peak width (0.11 µm) and height (0.02 µm), and valley depth (0.13 µm) and width (0.02 µm) compared with SS3 (peak width (0.14 µm) and height (0.04 µm) and valley depth (0.15 µm) and width (0.04 µm) of all the laser textured surfaces (Table 3). SS5 was also covered with rounded particles similar in structure to SS1 and SS2 (Fig. 5f). However, the nanostructure of SS5 was more rounded (Fig. 6f). The peak width (0.19 µm) and height (0.06 µm) and valley depth (0.12 µm) and width (0.02 µm) were smaller compared with SS1 and SS2 (Table 3). The size of each surface macro, micro and nano scale of surfaces was determined (Table 4). Regarding to laser generated topographies, it was clear that SS5 demonstrated the largest macro and micro size surface. SS1, SS2 and SS5 showed the largest nano features. SS4 had the smallest macro, micro and nano features with the exception of the control surface. For the nano topographies, surfaces SS1, SS2 and SS5 were overall significantly different to the other surfaces ($p > 0.05$).

Table 5 – Physicochemistry measurements for the modified stainless steel (mJ/m^2). Water contact angle standard deviations are in parenthesis.

	Water CA	ΔGiwi	γs	γsLW	γsAB	γs+	γs−
Control	80.9 ± 0.6	−59.1	42.1	38.6	3.4	1.1	2.8
SS1	157 ± 3.4	−67.9	6.8	2.9	3.8	1.0	3.8
SS2	160 ± 1.0	−99.7	2.1	1.2	0.9	0.2	1.1
SS3	148 ± 2.7	−33.6	19.4	14.6	4.9	0.6	10.1
SS4	99.6 ± 6.7	−74.0	24.9	24.0	0.9	1.2	0.2
SS5	154 ± 0.6	−91.4	3.2	1.6	1.5	0.5	1.3

3.1.3. *Physicochemistry*

The physicochemistry of the laser textured surface was characterised (Table 5). The control surface demonstrated the

Table 6 – Atomic percentages of elements in the surfaces detected by EDX (standard deviations are in parenthesis).

	Control	SS1	SS2	SS3	SS4	SS5
Fe	64.9 (0.1)	47.3 (1.1)	44.8 (0.9)	59.8 (1.2)	64.1 (1.5)	43.2 (0.5)
Cr	17.3 (0.1)	13.2 (0.5)	12.7 (0.3)	16.1 (0.4)	17.3 (0.4)	12.2 (0.2)
Ni	9.4 (0.1)	6.5 (0.1)	6.2 (0.1)	8.5 (0.3)	9.1 (0.2)	4.9 (1.6)
Mo	1.4 (0.1)	1.1 (0.1)	0.9 (0.0)	1.4 (0.1)	1.4 (0.1)	0.8 (0.0)
O	0.0 (0.0)	19.9 (0.5)	22.5 (0.6)	4.3 (0.5)	0.4 (0.5)	24.5 (0.8)
N	4.0 (0.1)	4.2 (2.1)	5.9 (0.4)	4.8 (1.8)	3.6 (1.3)	5.4 (0.6)
C	1.9 (0.0)	3.7 (0.5)	3.5 (0.3)	3.6 (0.3)	2.6 (0.4)	3.8 (0.4)
F	0.6 (0.1)	1.5 (0.4)	2.3 (1.3)	1.1 (0.3)	0.9 (0.6)	3.3 (1.3)
Si	0.6 (0.2)	1.1 (0.2)	1.0 (0.1)	0.7 (0.0)	0.4 (0.2)	0.9 (0.0)

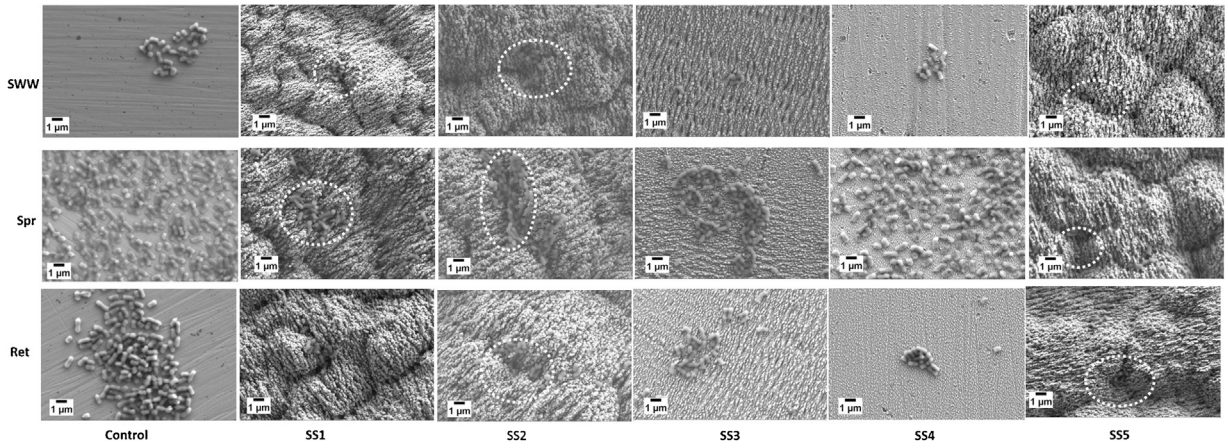

Fig. 7 – Distribution of the bacteria across the surfaces of different topographies and physicochemistries following the three assays Spray = Spr, SWW = spray with wash and Ret = retention. The eclipses highlight areas where bacteria have been retained.

greatest γ_s (42.1 mJ/m^2) and γ_s^{LW} (38.6 mJ/m^2) values which resulted in a less hydrophobic surface (ΔG_{iwi} −59.1 mJ/m^2). The most hydrophobic surfaces were found to have the greatest peak width and valley width topographies (ΔG_{iwi} SS2 −99.7 mJ/m^2 and SS5 −91.4 mJ/m^2). SS2 demonstrated the most superhydrophobic surface (ΔG_{iwi} −99.7 mJ/m^2) with the lowest surface values for all the parameters tested (γ_s. 2.1 mJ/m^2; γ_s^{LW} 1.2 mJ/m^2; γ_s^{AB} 0.9 mJ/m^2; γ_s^+ 0.2 mJ/m^2 and γ_s^- 1.1 mJ/m^2). SS5 was also demonstrated to have the lowest γ_s (3.1 mJ/m^2) and γ_s^{LW} (1.6 mJ/m^2) values. The least hydrophobicity surface was SS3 (ΔG_{iwi} −33.6 mJ/m^2) and this surface also demonstrated the greatest γ_s^{AB} (4.9 mJ/m^2) and γ_s^- (10.1 mJ/m^2) of all the surfaces produced. SS4 demonstrated surface characteristics similar to the control with high γ_s (24.9 mJ/m^2), γ_s^{LW} (24.0 mJ/m^2) and γ_s^+ (1.2 mJ/m^2) values and low γ_s^{AB} (0.9 mJ/m^2) and γ_s^- (0.2 mJ/m^2) values. All the results of the lasered surfaces for the contact angle, ΔG_{iwi}, γ_s, and γ_s^{LW} were significantly different from the control. For γ_s^{AB} the SS2, SS4 and SS5 surfaces were significantly different from the control, for γ_s^+, SS2, SS3 and SS5 were significantly different from the control and for γ_s, SS2, SS3, SS4 and SS5 were significantly different from the control ($p > 0.05$).

3.1.4. *Energy dispersive X-ray spectroscopy (EDX)*

Energy dispersive X-ray spectroscopy (Table 6) demonstrated that the chemical composition of the surfaces following laser treatment was as expected and consisted predominately of iron, with oxygen, nitrogen, chromium and nickel with some fluorine. Interestingly, the atomic fluorine levels for SS1 (1.47 at.%), SS2 (2.30 at.%) and SS5 (3.28 at.%) were higher than that obtained for SS3 (1.05 at.%) and SS4 (0.88 at.%). Since the X-ray penetration depth was about 1 μm–2 μm it was unlikely for fluorine to be found below the surface of the substrates. For the fluorine at.%, all the surfaces were significantly different to the control ($p > 0.05$).

3.2. *Microbiology*

The attachment, adhesion and retention of the bacteria was determined using three different microbiological assays (spray with wash, spray and retention). The SEM image of the *E. coli* bacteria attached on all the surfaces following all assays was demonstrated to show the distribution of the small amount of remaining cells on the surfaces (Fig. 7). It was clear that the bacteria were retained the grooves. A small number of bacteria were observed on all the surfaces following all the assays (Fig. 8). However, it was clear that following the attachment (spray with wash) assay that the greatest numbers of bacteria were retained on the control surface (1.1×10^5 cells/cm^2) then the SS4 surface (4.7×10^4 cells/cm^2), whereas, the lowest numbers were retained on SS5 (1.4×10^4 cells/cm^2). Following the adhesion (spray) assays, the greatest number of cells was retained on the control (8.1×10^5 cells/cm^2), then SS3 (2.3×10^5 cells/cm^2) with the least number of cells being retained on SS5 (8.8×10^4 cells/cm^2). Following the retention assay, the greatest numbers of cells were retained on the control surface (2.7×10^5 cells/cm^2) followed by the SS1 (1.0×10^5 cells/cm^2) with the least retained on SS5 (4.9×10^4 cells/cm^2). There was clearly a significant difference in all the assays for all the laser treated surfaces when compared to the control surfaces. SS5 showed the least numbers of bacteria following all the assays whilst the control showed the greatest numbers of bacteria. There was a significant difference in the number of bacteria retained on the control surface when compared to the number of bacteria retained on the laser etched surfaces for all the assays tested ($p > 0.05$).

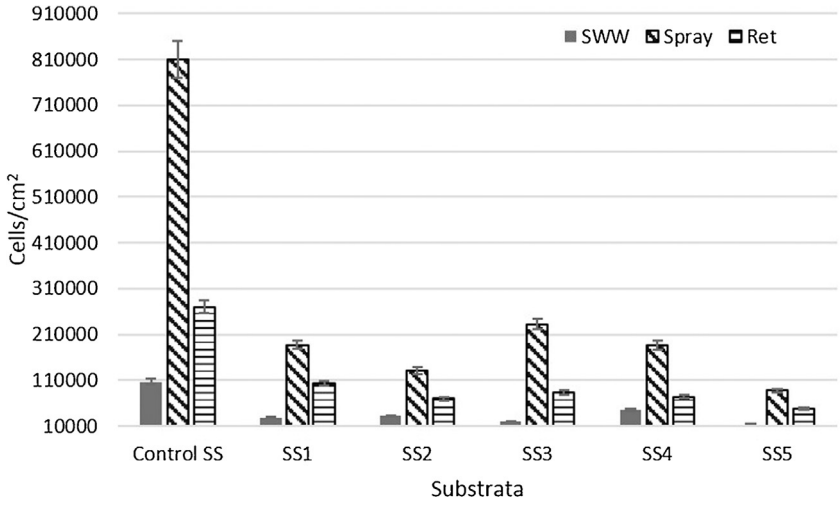

Fig. 8 – Average number of *E. coli* retained on stainless steel surfaces following three different assays, Spray, SWW = spray with wash and Ret = retention.

4. Discussion

4.1. *Laser surface treatment*

In the current work, Ps laser ablation was used to develop different hierarchical structures on 316L stainless steel surfaces. This occurs since during ultrashort laser interactions with metal surfaces, part of the lasers energy is absorbed by free electrons resulting in a thermalization process (Ben-Yakar et al., 2007). At the used speeds 1000 mm/s and 10 mm/s, the pulse overlapping in the direction of scanning speed was estimated from (Lehr and Kietzig, 2014);

$$pulse\ \ overlapping = \left(1 - \frac{speed}{repetitionrate * spot\ \ size}\right) \tag{7}$$

and was found to be 92.2%, and 99.92%. Therefore, the next pulse will interact with the hot surface due to the previous pulse. Taking into consideration the effect of hatch distances, there was also overlapping in the direction perpendicular to the scanning direction which was estimated using (Lehr and Kietzig, 2014);

$$line\ \ overlapping = \left(1 - \frac{\text{hatch distance}}{spot\ size}\right) \tag{8}$$

and was calculated to be, 20%, 60%, 92% and 95.4% using 100 μm, 50 μm, 10 μm and 10 μm respectively. Since the next laser pass was carried out over the area of the previous line a heat accumulation resulted in the production of different topographical structures. For the Laser Induced Periodic Surface Structures (LIPSS), there was a large amount of overlapping in both directions resulting in a considerable amount of laser intensity irradiating a small specific surface area which resulted in enhancement of the near field. Following the first pulse, the surface roughness and re-solidified particles can form. The fluence of the next pulse and next pass then becomes enhanced due to a nearfield mechanism. As a result, the following incident laser pulse reflection becomes increased, causing an enlarged energy deposition due to multiple laser beam absorption. If local overheating of the material occurs, in addition to material ablation, enhanced material melting can potentially take place. The structure of the circular forms covering the surface was therefore a result of the sintering of ablated materials together forming the particles (Li et al., 2015a). By changing the direction of scanning to 30°, the overlapping laser lines resulted in an increase in both of the surface average roughness and the height (peak to valley). When using a low laser fluence, high scanning speed and/or high hatch distances, ripples or LIPSS were produced. These ripples were different in their shapes; either cross ripples were produced with size of (~0.8 μm) covered with submicron features at low speed (10 mm/s) or pillars were produced when using high speed (1000 mm/s) and cross scanning direction. LIPPS formation has been intensively studied during the interaction of a femtosecond laser with metals and its formation depends on the laser fluence, modification of the threshold fluence, the polarization of incident light and laser induced surface instabilities (Wang and Guo, 2005; Bonse et al., 2012).

In this work, the physicochemistry of the surfaces was characterised. The surfaces were treated with FSA in order to stabilised the physicochemistry over time (>one month). All the manufactured surfaces were hydrophobic but there were differences in the degree of hydrophobicity. Taking into account the effect of laser parameters, it was found that the structures generated using very low speed and/or small hatch distance were hydrophobic with water contact angles >150°. The surfaces demonstrated hierarchical structures with increased roughness. This may be a result of the surface topographies resulting in increased air being trapped between the features thus increasing the hydrophobicity (Moradi et al., 2013; Long et al., 2014). However, it has been found that with increasing hatch distances and/or increasing scanning speed, the hydrophobicity was decreased. This might be attributed to the laser parameters; a decreased laser beam overlapping with increasing the hatch distances and increased scanning speed would result in decreasing the accumulated laser fluence irradiating the specific area which in turn results in the decreasing roughness (Lehr and Kietzig, 2014).

In this work, the Cassie–Baxter model was considered as the droplet of water did not wet the surface completely. Using the Cassie–Baxter model, the wettability is expressed as;

$$\cos\ \theta_r^c = f_1(\cos\ \theta_e + 1) - 1 \tag{9}$$

where f_1 and θ_e are the fraction of the solid in contact with the liquid and the intrinsic contact angle of the liquid droplet on the flat surface respectively (Cassie, 1948). Using this model, it can be predicted that by decreasing the value of f_1, an increase

in the value of θ_r^c should occur, independent of the value of θ_e. Thus, the larger fraction of air trapped within the interstices of the rough surface, the smaller the value of f_1 and the larger the apparent contact angle on the rough surface. All the laser generated structures showed an increased water contact angle of more than 18° in the case of using the fine LIPSS and more than 70° for the most hierarchical surfaces when compared with the control surface. The results also showed a decrease of ΔG_{iwi} of more than 30 mJ/m^2 for the hierarchical surfaces when compared with the control surface. The adsorption of FSA on the hierarchical treated surfaces also increased with increasing roughness resulting in more hydrophobic surfaces.

4.2. *Microbiology*

An understanding of how surface properties affect the attachment, adhesion and retention of bacteria may assist in designing or modifying the surfaces to discourage bacterial biofouling (Flint et al., 2000). The retention of bacteria on the surfaces depends on several factors such as surface topography, chemistry and surface wettability. The hierarchical ranges of surfaces roughness produced in this work showed that bacterial attachment, adhesion and retention was lower for the laser treated surfaces compared with the untreated surfaces. Overall, SS5 performed the best in all three assays; this surface had the widest peaks and values, but it was not the most superhydrophobic. However, it did have the greatest amount of adsorbed FSA. Its structures showed that it had the greatest macro grooves filled with smaller micro conical features covered by nanoparticles. The surfaces that retained the greatest number of bacteria were different for all three assays. All the surfaces that retained high numbers of bacteria (control, SS3 and SS4) demonstrated the lowest S_a, S_q and S_{pv} values. No single physicochemical value was found to be attributed to all the surfaces that retained the greatest bacterial numbers. Thus, the results suggest that superhydrophobic properties of a surface are not enough to impede fouling and such surface parameters need to be used in conjunction with defined, specific surface topographies and chemistries in order to reduce bacteria attachment adhesion and retention.

There are several studies carried out on to study the effect of superhydrophobic surfaces on bacterial adhesion using different substrates processed by different methods. Therefore, it is not surprising that contradictory results have been obtained. Li et al. (2015b) fabricated bio-mimic superhydrophobic surfaces with contact angles of 160° on polymer surfaces using nanoimprinting lithography techniques and reported that this surfaces was self-cleaning surfaces since *E. coli* adhesion was reduced by 60%. Our work demonstrated a greater bacterial reduction 89%, 87% and 82% on the SS5 surface following the adhesion, attachment and retention assays respectively. Recently, Dou et al. (2015) found that the adhesion of bacteria was significantly reduced on superhydrophobic bioinspired hierarchal structures duplicated from rose petal surfaces with a contact angle of ≥150° (Dou et al., 2015). Privett et al. (2011) also demonstrated that the adhesion of *Staphylococcus aureus* and *Pseudomonas aeruginosa* was significantly reduced on a superhydrophobic coating (water contact angle of 167°) obtained using fluorinated silica colloids (Privett et al., 2011).

Within this work, the surfaces with the greatest hydrophobicity was not found to be the most antiadhesive to the bacteria. However, SS5 was a superhydrophobic surface with $\Delta G_{iwi} = -91$ mJ/m^2. Surfaces produced in this work, all demonstrated surface free energy values of between 2.11 mJ/m^2–24.88 mJ/m^2 which were lower than the control surface. The effect of low surface free energy has been reported to reduce the adhesion of pathogens (Pereni et al., 2006), and the SS5 had a surface free energy of 3.17 mJ/m^2. The polar component of the surface free energy (γ^{AB}) has also been suggested to reduce the adhesion of bacteria when less than 5 mJ/m^2 (Harnett et al., 2007). However in our work, all the surfaces, including the control surface had γ^{AB} values of <5 mJ/m^2. In our work, the treated surfaces demonstrated generally lower γ_s^+ values than γ_s^- values (with the exception of SS4), confirming electron donor characteristics. This is in agreement with Rubio et al. (2002) and Santos et al. (2004) who demonstrated that the stainless steel was hydrophobic with electron donor characteristics.

5. Conclusions

This work generated hierarchical structures on stainless steel using a picosecond laser. This study showed that the surface roughness, feature geometry, chemistry and physicochemistry all interplayed to affect bacterial attachment, adhesion and retention. The surface that demonstrated the most antiadhesive properties was a hierarchal superhydrophobic surface with the greatest S_a and S_{pv} values, and the greatest peak and valley widths. Its structure had the greatest macro grooves filled with smaller micro conical features covered by nanoparticles, yet is was not the most superhydrophobic. This study reviled that picosecond laser surface texturing is a promising new method for producing different antiadhesive structures which may be useful in a range of applications.

Acknowledgement

The authors thank Iraqi Ministry of Higher Education and Scientific Research (MOHESR) for financial support of Fatema Rajab's PhD study.

References

Ben-Yakar, A., Harkin, A., Ashmore, J., Byer, R.L., Stone, H.A., 2007. Thermal and fluid processes of a thin melt zone during femtosecond laser ablation of glass: the formation of rims by single laser pulses. J. Phys. D: Appl. Phys. 40, 1447.

Bonse, J., Krüger, J., Höhm, S., Rosenfeld, A., 2012. Femtosecond laser-induced periodic surface structures. J. Laser Appl. 24, 042006.

Bos, R., Van der Mei, H., Gold, J., Busscher, H., 2000. Retention of bacteria on a substratum surface with micro-patterned hydrophobicity. FEMS Microbiol. Lett. 189, 311–315.

Cassie, A., 1948. Contact angles. Discuss. Faraday Soc. 3, 11–16.

Chou, S.Y., Krauss, P.R., Renstrom, P.J., 1995. Imprint of sub-25 nm vias and trenches in polymers. Appl. Phys. Lett. 67, 3114–3116.

Crick, C.R., Ismail, S., Pratten, J., Parkin, I.P., 2011. An investigation into bacterial attachment to an elastomeric superhydrophobic surface prepared via aerosol assisted deposition. Thin Solid Films 519, 3722–3727.

Cunha, A., Serro, A.P., Oliveira, V., Almeida, A., Vilar, R., Durrieu, M.-C., 2013. Wetting behaviour of femtosecond laser textured Ti–6Al–4V surfaces. Appl. Surf. Sci. 265, 688–696.

Cunha, A., Elie, A.-M., Plawinski, L., Serro, A.P., do Rego, A.M.B., Almeida, A., Urdaci, M.C., Durrieu, M.-C., Vilar, R., 2016. Femtosecond laser surface texturing of titanium as a method to reduce the adhesion of *Staphylococcus aureus* and biofilm formation. Appl. Surf. Sci. 360, 485–493.

Dantas, L.C.d.M., Silva-Neto, J.P.d., Dantas, T.S., Naves, L.Z., das Neves, F.D., da Mota, A.S., 2016. Bacterial adhesion and surface

roughness for different clinical techniques for acrylic polymethyl methacrylate. Int. J. Dent. 2016.
Dobrzański, L., Drygała, A., Gołombek, K., Panek, P., Bielańska, E., Zięba, P., 2008. Laser surface treatment of multicrystalline silicon for enhancing optical properties. J. Mater. Process. Technol. 201, 291–296.
Dou, X.-Q., Zhang, D., Feng, C., Jiang, L., 2015. Bioinspired hierarchical surface structures with tunable wettability for regulating bacteria adhesion. ACS Nano 9, 10664–10672.
Fadeeva, E., Truong, V.K., Stiesch, M., Chichkov, B.N., Crawford, R.J., Wang, J., Ivanova, E.P., 2011. Bacterial retention on superhydrophobic titanium surfaces fabricated by femtosecond laser ablation. Langmuir 27, 3012–3019.
Flint, S., Brooks, J., Bremer, P., 2000. Properties of the stainless steel substrate, influencing the adhesion of thermo-resistant streptococci. J. Food Eng. 43, 235–242.
Gold, J., Nilsson, B., Kasemo, B., 1995. Microfabricated metal and oxide fibers for biological applications. J. Vac. Sci. Technol. A 13, 2638–2643.
Green, A.M., Jansen, J.A., Van der Waerden, J., Von Recum, A.F., 1994. Fibroblast response to microtextured silicone surfaces: texture orientation into or out of the surface. J. Biomed. Mater. Res. 28, 647–653.
Harnett, E.M., Alderman, J., Wood, T., 2007. The surface energy of various biomaterials coated with adhesion molecules used in cell culture. Colloids Surf. B: Biointerfaces 55, 90–97.
Hilbert, L.R., Bagge-Ravn, D., Kold, J., Gram, L., 2003. Influence of surface roughness of stainless steel on microbial adhesion and corrosion resistance. Int. Biodeterior. Biodegrad. 52, 175–185.
Jullien, C., Bénézech, T., Carpentier, B., Lebret, V., Faille, C., 2003. Identification of surface characteristics relevant to the hygienic status of stainless steel for the food industry. J. Food Eng. 56, 77–87.
Lehr, J., Kietzig, A.-M., 2014. Production of homogenous micro-structures by femtosecond laser micro-machining. Opt. Laser. Eng. 57, 121–129.
Li, Y., Cui, Z., Wang, W., Lin, C., Tsai, H.-L., 2015a. Formation of linked nanostructure-textured mound-shaped microstructures on stainless steel surface via femtosecond laser ablation. Appl. Surf. Sci. 324, 775–783.
Li, Y., John, J., Kolewe, K.W., Schiffman, J.D., Carter, K.R., 2015b. Scaling up nature—large area flexible biomimetic surfaces. ACS Appl. Mater. Interfaces 7, 23439.
Long, J., Fan, P., Zhong, M., Zhang, H., Xie, Y., Lin, C., 2014. Superhydrophobic and colorful copper surfaces fabricated by picosecond laser induced periodic nanostructures. Appl. Surf. Sci. 311, 461–467.
Long, J., Fan, P., Gong, D., Jiang, D., Zhang, H., Li, L., Zhong, M., 2015a. Superhydrophobic surfaces fabricated by femtosecond laser with tunable water adhesion from lotus leaf to rose petal. ACS Appl. Mater. Interfaces 7 (18), 9858–9865.
Long, J., Zhong, M., Fan, P., Gong, D., Zhang, H., 2015b. Wettability conversion of ultrafast laser structured copper surface. J. Laser Appl. 27, S29107.
Long, J., Pan, L., Fan, P., Gong, D., Jiang, D., Zhang, H., Li, L., Zhong, M., 2016. Cassie-state stability of metallic superhydrophobic surfaces with various micro/nanostructures produced by a femtosecond laser. Langmuir 32, 1065–1072.
Milledge, J.J., 2010. The cleanability of stainless steel used as a food contact surface: an updated short review. Food Sci. Technol. J. 24, 27–28.
Moradi, S., Kamal, S., Englezos, P., Hatzikiriakos, S.G., 2013. Femtosecond laser irradiation of metallic surfaces: effects of laser parameters on superhydrophobicity. Nanotechnology 24, 415302.
Nyachuba, D.G., 2010. Foodborne illness: is it on the rise? Nutr. Rev. 68, 257–269.
Pereni, C., Zhao, Q., Liu, Y., Abel, E., 2006. Surface free energy effect on bacterial retention. Colloids Surf. B: Biointerfaces 48, 143–147.
Perera-Costa, D., Bruque, J.M., Gonzaílez-Martiín, M.a.L., Gómez-García, A.C., Vadillo-Rodriguez, V., 2014. Studying the influence of surface topography on bacterial adhesion using spatially organized microtopographic surface patterns. Langmuir 30, 4633–4641.
Privett, B.J., Youn, J., Hong, S.A., Lee, J., Han, J., Shin, J.H., Schoenfisch, M.H., 2011. Antibacterial fluorinated silica colloid superhydrophobic surfaces. Langmuir 27, 9597–9601.
Rubio, C., Costa, D., Bellon-Fontaine, M., Relkin, P., Pradier, C., Marcus, P., 2002. Characterization of bovine serum albumin adsorption on chromium and AISI 304 stainless steel, consequences for the *Pseudomonas fragi* K1 adhesion. Colloids Surf. B: Biointerfaces 24, 193–205.
Santos, O., Nylander, T., Rosmaninho, R., Rizzo, G., Yiantsios, S., Andritsos, N., Karabelas, A., Müller-Steinhagen, H., Melo, L., Boulangé-Petermann, L., 2004. Modified stainless steel surfaces targeted to reduce fouling—surface characterization. J. Food Eng. 64, 63–79.
Schlisselberg, D.B., Yaron, S., 2013. The effects of stainless steel finish on *Salmonella typhimurium* attachment, biofilm formation and sensitivity to chlorine. Food Microbiol. 35, 65–72.
Srey, S., Jahid, I.K., Ha, S.-D., 2013. Biofilm formation in food industries: a food safety concern. Food Control 31, 572–585.
Tetlow, L.A., Lynch, S., Whitehead, K.A., 2017. The effect of surface properties on bacterial retention: a study utilising stainless steel and TiN/25.65 at.% Ag substrata. Food Bioprod. Process. 102, 332–339.
Van Oss, C., Ju, L., Chaudhury, M., Good, R., 1989. Estimation of the polar parameters of the surface tension of liquids by contact angle measurements on gels. J. Colloid Interface Sci. 128, 313–319.
Verran, J., Packer, A., Kelly, P., Whitehead, K.A., 2010. The retention of bacteria on hygienic surfaces presenting scratches of microbial dimensions. Lett. Appl. Microbiol. 50, 258–263.
Wang, J., Guo, C., 2005. Ultrafast dynamics of femtosecond laser-induced periodic surface pattern formation on metals. Appl. Phys. Lett. 87, 251914.
Wang, H., Feng, H., Liang, W., Luo, Y., Malyarchuk, V., 2009. Effect of surface roughness on retention and removal of *Escherichia coli* O157:H7 on surfaces of selected fruits. J. Food Sci. 74.
Whitehead, K.A., Verran, J., 2006. The effect of surface topography on the retention of microorganisms. Food Bioprod. Process. 84, 253–259.
Whitehead, K., Verran, J., 2009. The Effect of Substratum Properties on the Survival of Attached Microorganisms on Inert Surfaces. Marine and Industrial Biofouling. Springer, pp. 13–33.
Whitehead, K.A., Colligon, J., Verran, J., 2005. Retention of microbial cells in substratum surface features of micrometer and sub-micrometer dimensions. Colloids Surf. B: Biointerfaces 41, 129–138.
Whitehead, K., Benson, P., Verran, J., 2011. The detection of food soils on stainless steel using energy dispersive X-ray and Fourier transform infrared spectroscopy. Biofouling 27, 907–917.
Whitehead, K., Benson, P., Verran, J., 2015. Developing application and detection methods for *Listeria monocytogenes* and fish extract on open surfaces in order to optimize cleaning protocols. Food Bioprod. Process. 93, 224–233.
Yan, Y.Y., Gao, N., Barthlott, W., 2011. Mimicking natural superhydrophobic surfaces and grasping the wetting process: a review on recent progress in preparing superhydrophobic surfaces. Adv. Colloid Interface Sci. 169, 80–105.